Implementation of Digital Image processing in Calculating Normal Approach for Spherical Indenter Considering Elastic/Plastic Contact

Rana Abdul Rahman Lateef and **Ahmed Abdul Hussein**
Baghdad college of economics **university of Baghdad**
Science university **mech. engineering department**
Dep. Of computer science

Abstract:

In this work a study and calculation of the normal approach between two bodies, spherical and rough flat surface, had been conducted by the aid of image processing technique. Four kinds of metals of different work hardening index had been used as a surface specimens and by capturing images of resolution of 0.006565 mm/pixel a good estimate of the normal approach may be obtained the compression tests had been done in strength of material laboratory in mechanical engineering department, a Monsanto tensometer had been used to conduct the indentation tests.

A light section measuring equipment microscope BK 70x50 was used to calculate the surface parameters of the texture profile like standard deviation of asperity peak heights, centre line average, asperity density and the radius of asperities.

A Gaussian distribution of asperity peak height was assumed in calculating the theoretical value of the normal approach in the elastic and plastic regions and where compared with those obtained experimentally to verify the obtained results.

الخلاصة:

في هذا البحث تم دراسة التقارب العمودي بين جسمين ، كروي وسطح مستوي خشن، باستخدام تقنية المعالجة الصورية . أربع انواع من المعادن أستخدمت كل منها له معامل تصليد بالتشغيل مختلف عن الآخر لأجل استخدامها كعينات سطوح، ومن خلال ألتقاط صور بدقة 0.006565ملم لكل نقطة ضوئية(pixel) يمكن حساب التقارب العمودي بدقه مقبوله. اختبار الضغط تم اجراءه في مختبر مقاومة المواد في قسم الهندسه الميكانيكيه وباستخدام جهاز (tenso-meter Monsanto) تم أجراء فحص الخرق .

أستخدم جهاز ميكروسكوب قياس الأسقاط المقطعي (BK.70X50) في ايجاد متغيرات ومواصفات السطح مثل الأنحراف المعياري لأرتفاعات النتؤات ومعدل الخط المركزي وكثافة النتؤات وكذلك أنصاف أقطارها.

تم افتراض التوزيع العشوائي لأرتفاع النتؤات في أحتساب القيم النظرية للتقارب العمودي في منطقتي المرونه واللدونه وتمت مقارنتها مع تلك المحسوبه عملياً.

Introduction:

Digital image correlation (DIC) is a non –contacting measuring technique that has been developed to obtain full field surface displacements and their gradients (strains) of objects under stress. The DIC method has evolved over the last decade and its usefulness for measuring small displacements as occurs in engineering materials in tension and compression has been demonstrated by several investigators. The theory of digital image correlation has been described in detail by several researchers but a detailed treatment of the subject can be found in Sutton etal, 1983 the underling principle of DIC and its application to obtain displacement fields can be found in Samarasingle and kvlasiri, 2000.

All surfaces are microscopically rough. Therefore when two surfaces are in contact the load is borne by the discrete spots at the tip of surface asperities and the real contact area is only a small function of the apparent contact area.

The phenomena of contact surfaces are of fundamental importance in the study of tribology and other applications [Halling, J and Nuri.K.A 1988]. Therefore there have been numerous efforts to relate surface roughness to the stresses and deformation when two surfaces are pressed together. The Hertz elastic contact mechanics governs the deformation of each asperity. An experimental study conducted by Powierza et.al.1992 verified the theoretical results of the Greenwood model for elastic deformation and for isotropic surfaces. However, when there are substantial amount of asperities deformed plastically the theoretical results deviate distinctly from the experimental data.

Several investigations have been conducted to deal with the plastic deformation of asperities Pullen and Williamson 1972 showed that for the plastic deformation of asperities, volume is conserved by a uniform rise in the non-contacting part of the surface.Results from finite element analysis performed by Kucharski et.al. 1994 for an asperity with elasto-plastic deformation agree well with the observation of Pullen and Williamson. Zhao etal.2000 proposed a model that considers the continuity and smoothness of variables across different modes of deformation. Their results show that this model is more complete in describing the contact of rough surfaces and is consistent with experimental observation and physical intuition.

The deformational models deal with rough surfaces with isotropic contacts. However rough surfaces can have elliptical contacts because engineering surfaces have asperities with various curvatures for various directions.

The present study propose a spherical micro contact model taking in account the elastic, elsto-plastic and fully plastic deformation.

In the proposed model, every asperity is assumed to have the same radii just as Greenwood model like many other models which assume that all asperities are circular. The proposed model is useful for surface with a pronounced grain in one direction.

Analysis Based on Constant Indenter Radius

It is necessary to define the normal approach of a sphere to the normal load and the consequent deformation, considering the contact of a sphere and a plane, fig.1.
It is easily seen that the separation u of the surfaces at a distance r from the centre of the contact zone is given by

$$u = R - (R^2 - r^2)^{1/2} = R - R\left(1 - \frac{r^2}{R^2}\right)^{1/2} = R - R + \frac{r^2}{2R} + \cdots$$

If r is small compared to R then

$$u = \frac{r^2}{2R}$$

If a is the radius of the contact zone and w is the displacement of the sphere at the boundary of this zone then the normal approach δ will be given by

$$\delta = u + w = \frac{a^2}{2R} + w$$

At the center of the contact zone δ is given by the degree of deformation and it is therefore reasonable to assume that the normal approach will be proportional to the flattening of the sphere. In other words

$$\delta \propto \frac{a^2}{R}$$

From the results given by Hertzian contact [Halling J. 1975]

$$a \propto \left(\frac{N R}{\acute{E}}\right)^{1/3} \quad or \quad a = \left(\frac{3}{4}\frac{N \acute{R}}{\acute{E}}\right)^{1/3}$$

Where $\frac{1}{\acute{E}} = \frac{1-v_1^2}{E_1} + \frac{1-v_1^2}{E_2}$

So that $\delta \propto \left(\frac{N^2}{\acute{E}^2 R}\right)^{1/3}$

The exact result show that [Halling J. 1975]

$$\delta = \left(\frac{9N^2}{16\acute{E}^2 R}\right)^{1/3}$$

Or $N = \frac{4}{3}\acute{E}\, R^{1/2}\delta^{3/2}$

The area of contact, A , will be given by

$$A = \pi a^2 = \pi R \delta$$

The theoretical analysis employed in the present work for determining the load-normal approach relationship of a sphere in contact with a rough plane is based on the model shape of the rough surface as shown in fig.2.

In this figure the flat surface is considered to be covered with similar asperities having randomly varying heights. The chosen asperity peak heights form a small sample from a large population of a random deviate following the Gaussian distribution about a mean plane, and the asperities are assumed to be spherical caps all with the same radius.

The elastic deformation of the surfaces will be neglected and the asperities will be assumed to deform with ideal plastic mode under a constant flow pressure. Each individual load will be taken as a point force acting on a semi-infinite plane and the collective effect of these forces is then considered

We shall use the results which ensue from the contact of a sphere of a material having a stress strain behavior of the form

$$\bar{\sigma} = B\bar{\epsilon}^n \quad (1)$$

Where $\bar{\sigma}$ and $\bar{\epsilon}$ are the effective stress and strain values based on the assumption that the strain ratios are constant and that the principal axes do not rotate. This is admissible for spherical contacts if we assume a geometrical similarity of contact with its scale being defined simply by the size of the contact radius. Thus, [William F. Hosford1983]

$$\bar{\sigma} = \left[{}^1/_2 \, (\sigma_1 - \sigma_2)^2 + (\sigma_2 - \sigma_1)^2 + (\sigma_3 - \sigma_1)^2 \right]^{1/2} \quad (2)$$

$$\bar{\epsilon} = {}^1/_3 \left[2\,(\epsilon_1 - \epsilon_2)^2 + (\epsilon_2 - \epsilon_3)^2 + (\epsilon_3 - \epsilon_1)^2 \right]^{1/2} \quad (3)$$

It is apparent that the $\bar{\sigma}$ is the yield stress in simple tension and that when n=0 the material behaves in a perfectly plastic fashion and B is the constant yield stress, Y. When n=1 the behavior may be considered as perfectly elastic and $B = E/(1+\nu)$.

For the contact of a material defined by eq. (1) with a rigid sphere of the same size we shall assume that $\bar{\sigma}$ is a linear function of the contact pressure, thus.

$$\bar{\sigma} = \frac{1}{c} \frac{p}{\pi a^2} \quad (4)$$

Where p is the load, a is the radius of the contact zone and c is a constant. For metals it is known that c has a value of about 2.8 being the relation between the current yield stress and the current hardness of the material, see fig.3.[Halling J. 1975]

The strain must be some function of α/β where β is the radius of the sphere. Expanding such a function as a power series and, since $\beta \gg a$, neglecting all but the first term gives,

$$\bar{\epsilon} = D\frac{a}{\beta} \quad (5)$$

Where D is some unknown constant. Combining eqn. (1), (4) and (5) yields

$$P\,\beta_{1/2}^{n} = K\alpha^{(2+n)} \quad (6)$$

Whence

$$\frac{K}{B} = \pi\, c\, D^n \quad (7)$$

We would therefore anticipate that K/B would be a constant for a given material characteristic n. Known solutions to eqn. (6) are the elastic case when n=1 and $K_e = 4/3\ \acute{E}$ where, $1/E' = (1 - \nu\text{^}2)/E$

And the perfectly plastic case when n=0 and $K_p = \pi H$ where H is the indentation hardness of the material. Equation (5) may now be written,

$$\bar{\epsilon} = \left(\frac{K}{\pi B c}\right)^{1/n} \left(\frac{a}{\beta}\right) \quad (8)$$

Finally we shall be interested in the normal approach δ of a loaded sphere so that we shall assume a relationship of the form,

$$a^2 = \lambda\beta\delta \qquad (9)$$

Since we know that $\lambda = 1$ for the elastic case when n=1 and $\lambda = 2$ for the perfectly plastic case when n=0. Equation (8) may be written in the more useful form.

$$\bar{\epsilon} = \left(\frac{K}{\pi Bc}\right)^{1/n}\left(\frac{\lambda\delta}{\beta}\right)^{1/2} \qquad (10)$$

In the foregoing sequence of equations we note that we require a knowledge of such constant as *c,B,n,K* and λ. These constants are determined in ref.[Halling J. 1975] and from those results may obtain the empirical relationship

$$\frac{K}{B} = \pi \cdot c(1 - 0.9n)$$

Or $$D = \frac{K}{\pi Bc} = (1 - 0.9n) \qquad (11)$$

The variation of λ for materials with various values of *n* may be obtained from the empirical expression mentioned in ref. [Halling J. 1975] which is shown in fig.5 [Halling J. 1975].

$$\lambda = 2 - n^{1/2} \qquad (12)$$

The Contact of Rough Surfaces

Consider a surface containing a point distribution of rigid spherical asperities against a rough surface consisting of an array of spherical asperities of a material defined by eq.(1). All the asperities are assumed to be spherical of radius $\beta$and it is tacitly assumed that an asperity on the upper surface is aligned with each asperity on the rough surface, Fig. (2). Following the arguments used by Greenwood and Williamson, but using the foregoing results we may define each discrete area of contact $A_i$as, [Powierza Z.H. et.al. 1992]

$$A_i = \lambda\pi R\delta = \pi a^2 \qquad (13)$$

Using eqns(6) and (9) defines the load at any contact as

$$P_i = K\lambda^{\left(1+\frac{n}{2}\right)}\delta^{\left(1+\frac{n}{2}\right)}\beta^{1-\frac{n}{2}} \qquad (14)$$

Let the surfaces be separated by a distance *d* at any total load P where d is measured from some datum in the rough surface to the tips of the rigid spherical asperities. For any contacting asperity on the rough surface of initial height *z* above the datum the normal approach will be $= z - d$. The probability of contact for any asperity of height z is,

$$prob.(z > d) = \int_d^\infty \varphi(z) \cdot dz \qquad (15)$$

Where $\Phi(z)$ is the probability function of the heights and the number of asperity contacts will be,

$$N\int_d^\infty \Phi(z)dz \qquad (16)$$

N being the total number of asperities within the contact region. The total real area of contact A and the total load P thus become.[Nuri K.A. 1974]

$$A = \lambda\pi\beta N\int_d^\infty (z - d)\Phi(z)dz \qquad (17)$$

$$P = K\lambda^{1+\frac{n}{2}}\beta^{1-\frac{n}{2}}N\int_{d}^{\infty}(z-d)^{1+\frac{n}{2}}\Phi(Z)dz \quad (18)$$

Equation (17) and (18) reduce to the well known solution for the spherical case of *n=0* and *n=1*, i.e. perfectly plastic or perfectly elastic contact.

Point Detection in Image Processing:

Digital image detection is a measuring technique has been used to obtain full field surface displacements. This is done by applying two white points on the specimens under test and applying the point detection technique on the image of interest, according to this a distance or a displacement between these two points are calculated using Euclidean distance between two n-dimensional (row or column) vector x and y to evaluate the normal approach between the spherical smooth surface and rough flat surface.

In this work, an image with size (2700 × 2300) pixel JPEG format has been captured by a Ginex CCD (charge Couple Device) video camera and a lens with ×8 magnifications.

A calibration process has been done to estimate the precision of the measurement by capturing picture for bodies with defined dimension.

The result shows that a precision of 152 pixels per 1 mm have been achieved, this equals to 0.006565 mm/pixel.

Experimental Procedure:

Four kinds of test metals had been used in this work namely steel ck45, Aluminum and two types of Brass. Their chemical composition analysis is given in table (1).

The test specimens were polished with emery paper having different grades 200,400 and 600 to have their surfaces smooth, those specimens where fully annealed in an oven under the temperature of $650C^0$ for steel , $550C^0$ for Brass and $400C^0$ for Aluminum for about 1.5 hour. The specimens were kept in the oven for one day to cool down slowly and evenly to room temperature. The annealing process had been done in the mechanical engineering laboratory for metals.

A Monsanto tensometer had been used where a hand driven gear box of high mechanical advantage applies a force of up to 20kN to the test piece. The tensometer can be used for compression and indentation tests simply by using the compression cage shown in fig (6)

Precision alignment enables the dies used for the compression to be mounted directly to the tables of the compression cage.

For many ductile metals which have not been cold worked prior to the tensile test (i.e. that are fully annealed) the behavior from initial yield to ultimate load is adequately described by an expression of the form [William F. Hosford 1983]

$$\sigma = B\,\epsilon^{n} \quad (19)$$

Where for an induced strain ϵ, the corresponding value of σ is the new yield strength caused by the degree of

cold working that induced the strain . The tensile results are, in fact, descriptive of an effective stress-strain plot. For that reason eq(19) can be written as

$$\bar{\sigma} = B\bar{\epsilon}^{n} \qquad (20)$$

The numerical values of B and n are determined in ref. [Ahmed A.A. 1993] where the same test specimens had been used in this work. The following relation ships were found to correlate with the experimental results

Steel ck 45 $\bar{\sigma} = 2387.76\ \bar{\epsilon}^{0.73085}$

Brass1
$\bar{\sigma} = 691.498576\ \bar{\epsilon}^{0.43764}$

Brass 2 $\bar{\sigma} = 545.8925\ \bar{\epsilon}^{0.5336}$

Aluminum
$\bar{\sigma} = 184.7311\ \bar{\epsilon}^{0.25456}$

Alight section measuring equipment (microscope BK70X50) shown in fig. (7) had been used to measure tip heights of asperities for the specimens under test. The BK 70x50 measuring microscope operates on the basis of Pof-schamaltz light section method. A thin light strip is brought to section at 45^0 with the horizontally arranged surface to be measured so that the generated profile of intersection between light strip and surface to be checked becomes visible, the visible light strip had been captured using digital camera with a resolution of 7 megapixel a sample of this picture are shown in fig. (8)

Lenses of magnification of 30x12.5 had been used in BK 70x50 microscope which enable to capture photos with precession of 0.00004347 mm/pixel and with lenses of 60x12.5 a precession of 0.0000224 mm/pixel may be achieved . The first set of lenses had been used to study the surface texture height and distribution while the second set of lenses is used to calculate the radios of asperities for the various test specimens surfaces.

A Hough transform method for edge detecting and linking had been applied on images obtained from microscope BK 70x50, to detect the tips and valleys of the rough surface in the test specimens.

A Hough transform in this work used to detect curves or peaks. Because of the quantization in space of the digital images, the quantization in parameter space of Hough transform as well as the fact that edges in typical images are not perfectly straight. Hough transform peaks tend to lie in more than Hough transform cell.

The algorithm or the strategy is as follows:

1- Find the Hough transform cell containing the highest value and record its location.
2- Suppress (set to zero) Hough transforms cells in the immediate neighborhood of the maximum found in step 1.
3- Repeat until the desired number of peaks has been found, or until a specified threshold has been reached.

Once a set of candidate peaks has been identified in Hough transform, it remains to be determined if there are line segments associated with those peaks, as well as where they start and end. For each peak, the first step is to find the location of all nonzero pixels in the image that contributed to that peak.

As the pixels associated with the location found it must be grouped into line segments with the following steps:

1- Rotate the pixel locations by $90^0 - \theta$ so that they lie approximately along a vertical line.
2- Sort the pixel location by their rotated *X*-values.
3- Merging adjacent line segments. That is separated by a small space.

The procedure for obtaining the normal approach in this work experimentally is based on taking several images for the two approaching bodies (spherical and specimen) using LCD camera for each step of loading with a resolution of 0.006565mm/pixel and by calculating the distance between two specific points one on the specimen and the other on the spherical indenter, for each loading case, the normal approach between the approaching bodies may be specified.

Calculating the normal approach is based on the application of Euclidean distance between two points which is defined as [Gonzalez R. C. 2008]

$$D_e(p,q) = [(x-s)^2 + (y-\tau)^2]^{1/2}$$

Where *(x,y)* are the coordinates of the two pixels *p* and *q* so, by taking arbitrary two points each of lies on one of the approaching bodies the distance between these points are calculated using the equation mentioned above.

The distance between those points in the first image for the case of no load is compared with the other cases for the step loading and the difference between the distances for each step of loading is compared with the first case of no load. A typical kind of the images used in calculating the normal approach is shown in fig.(9)

Results and Discussion:

From the analyzed images of the four test specimens may obtain the parameters shown in table 2 which are used in calculating the theoretical relation between the applied load and deformation (normal approach) which were used for comparison with the experimental results. A Gaussian distribution of asperity heights had been assumed in plotting theoretical curves with a limit of 3σ, those curves are shown in figs.(10-17). Two steel balls of diameter 10mm and 5mm had been used in the indentation tests for calculating normal approach the results of tests for the four kinds of metals used are shown as crosses in figures (10-17).

In figs. (10-17) the normal approach for 5mm diameter spherical indenter is bigger than for 10mm diameter sphere having the same load, this is due to the high pressure at the contact zone which causes deformation of asperities.

Metals that have low work hardening index, like aluminum, deforms plastically compared with those having higher work hardening index, like steel, at the same load as shown in fig.(10-17) where the normal approach decreases while the work hardening index increases for the same load.

Surfaces having a high center line average (C.L.A.) of asperity height and high standard deviation of all ordinate height deformed more than those having lower C.L.A. and lower standard deviation as shown when comparing between fig.(12) and fig.(14) for 10mm diameter indenter and between fig.(13) and fig.(15) for 5mm diameter indenter

Conclusions:

Experimental results seems to lie between the theoretical curves of elastic and plastic regions even though the load applied is higher than the load needed for plastic deformation which means that the theoretical analysis for predicting the normal approach did not conform the experimental results. These results agree with the work of Powerza et.al. 1992 where in their experimental study they showed that when there are substantial amount of asperities deformed plastically the theoretical results deviate distinctly from experimental data.

The predicted theoretical elastic and plastic region limits depend on the assumed kind of distribution of asperity height which is assumed here as Gaussian distribution , this assumption plays a big rule in the deviation of the experimental results from the bands of elastic and plastic limits although most of the experimental results at high loads lie within those bands.

References:

Ahmed A.A. " Contact mechanics of rough engineering surfaces" a thesis submitted to the college of engineering university of Baghdad 1993.

Halling J. , and Nuri K.A. 1988 , "the elastic – plastic contact of rough surfaces and its relevance in the study of wear" Proc. Inst. Mech. Eng. Part c; J. Mech. Eng. Sci., 202(c4)pp. 269-274.

Halling J. "A contribution to the theory of mechanical wear" 1975,wear,34,pp239-249.

Halling J. "Principles of tribology" 1975, Macmillan press LTD.

Kucharski S., Kilmezak T., Palijanink J. and Kaczmarck J., 1994 " Finite element model for the contact of rough surfaces." Wear 177,pp1-13.

Nuri K.A., 1974, " The normal approach between curved surfaces in contact" Wear,30,pp.321-335.

Powierza Z.H., Klimezak T., and Polijanink A., 1992, " On the experimental verification of the Greenwood-Williamson model for the contact of rough surface" Wear,154,pp. 115-124.

Pullen J.,and Williamson J.B.P., 1972 " On the plastic

of rough surface" Proc. R. Soc. London Ser. A: A327 pp159-173.

Rafael C. Gonzalez , Richard E. Woods and Steven L. Eddins"digital image processing using Matlab" 2004, Pearson international edition.

Rafael C. Gonzalez and Richard E. Woods "digital image processing" 2008, Pearson international edition, third edition.

Samarasingle S., & Kvlasiri,G.D. 2000, displacement fields of wood in tension based on image processing . Silva Fennica 34(3);251-273.

Sutton , M.A., Wolters , W.J., Peters, W.H., Rawson , W.F. & Mc Neill, S.R., 1983, Determination of displacements using an improved digital image correlation method. Image and vision computing 1(3); 133-139.

William F. Hosford and Robert M. Caddel " Metal forming mechanics and metallurgy" 1983,Prentice-Hall, Inc., Englewood Cliffs

Zhao Y., Maietia D.M. , and Chi I. , 2000 " An asperity micro contact model incorporating the transition from elastic deformation to fully plastic flow."ASME, J., Tribol., 122(1),pp.86-93.

Nomenclatures

symbol	definition	units
u	Separation of the surfaces	mm
a	Radius of contact zone	mm
R	Radius of sphere	mm
δ	Normal approach	mm
A	Area of contact	Mm^2
β	Radius of asperity	mm
$\bar{\sigma}$	Effective stress	N/mm^2
$\bar{\epsilon}$	Effective strain	-
n	Work hardening index	-
p	load	N
υ	Poisons ratio	-
λ	Area factor	-
$\Phi(z)$	Probability function of height distribution	-
N	Total number of asperities within the contact zone	-

Table(1) chemical composition analysis of test specimens

Comp.	Steel ck45	Aluminum	Brass 1	Brass 2
C	0.42-0.5			
Si	0.15-0.35	0.235		
Mn	0.5-0.8	0.007		0.012
P	<0.035			
S	<0.035			
Cr				0.004
Fe	Remainder	0.174	0.021	2.333
Zn		0.008	0.192	26.31
Pb		0.003	21.69	
Mg		0.444		
Cu		0.013	remainder	69.45
Ni			0.351	0.069
Al		remainder		

Table(2) surface parameters obtained by image processing analysis

	Aluminum	Brass 1	Brass 2	Steel ck45
Density η asp./mm^2	255.178	399.408	175.78	285.714
Standard deviation of all height $\sigma \times 10^{-3} mm$	5.617	7.75	2.079	3.812
Radius of asperities $\beta \times 10^{-3} mm$	2.402	0.6207	1.741	0.5703
Center line average C.L.A. $\times 10^{-3}$	4.56978	5.71246	1.55	3.21147

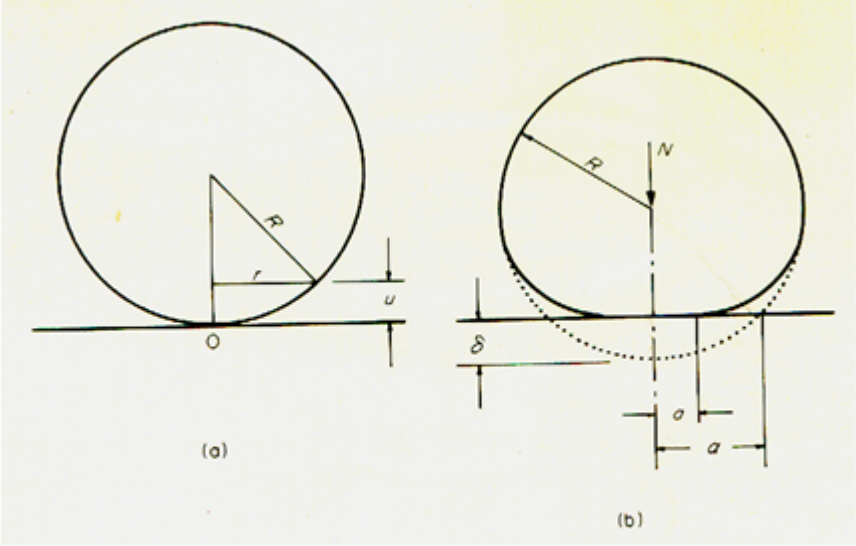

Fig(1) Elastic contact between a sphere and a plane [Halling J. 1975]

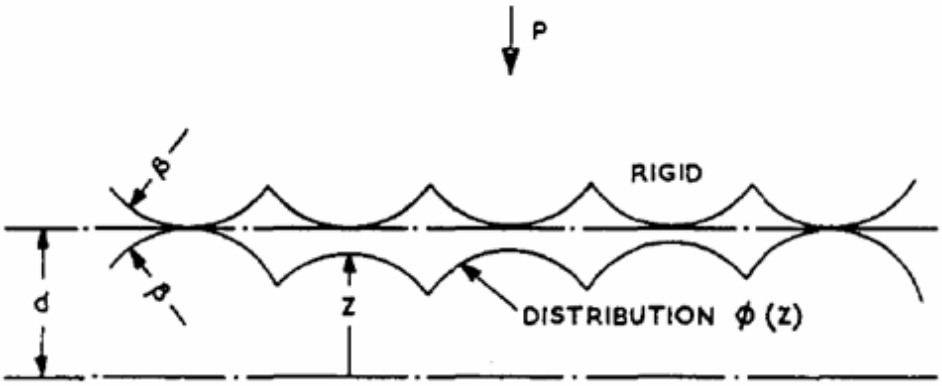

Fig.(2) Normal contact of rough surfaces.

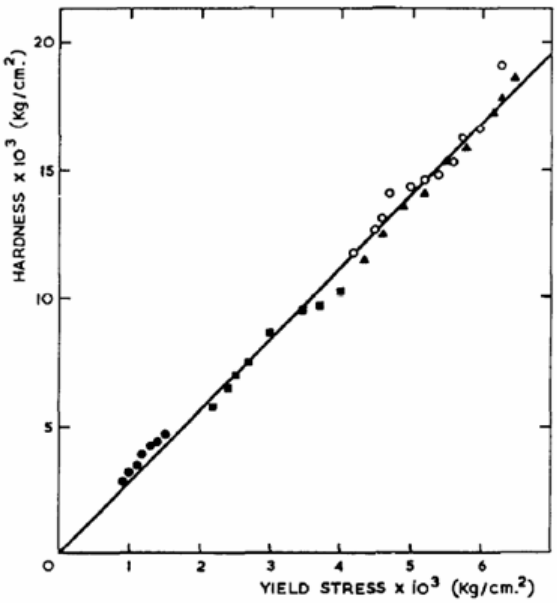

Fig.(3) Variation of the hardness with yield stress for various metals, · aluminum, ■ copper, *o* brass, Δ mild steel

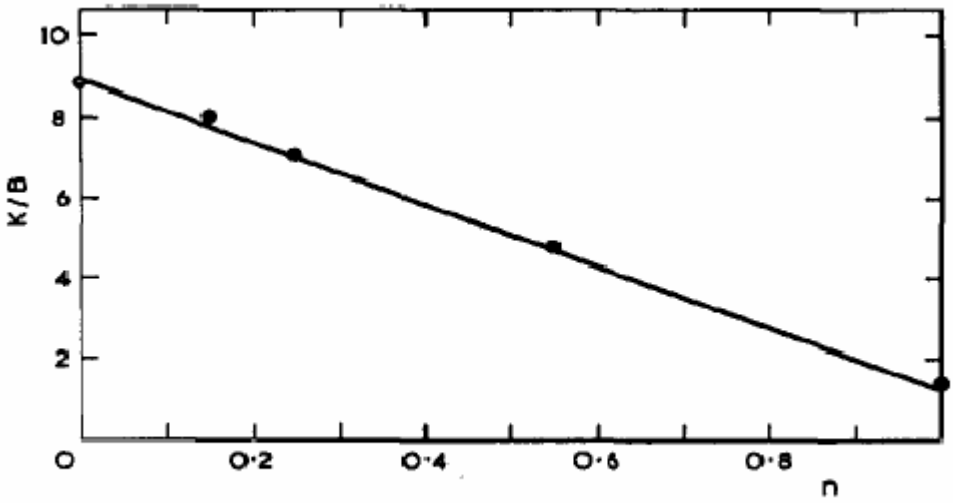

Fig(4) Variation of K/B with degree of work hardening [3]

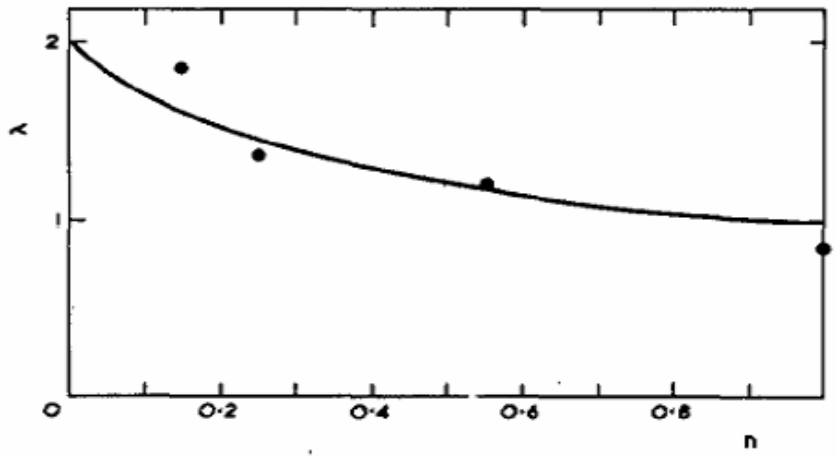

Fig.(5) Variation of the area factor with degree of work hardening. [3]

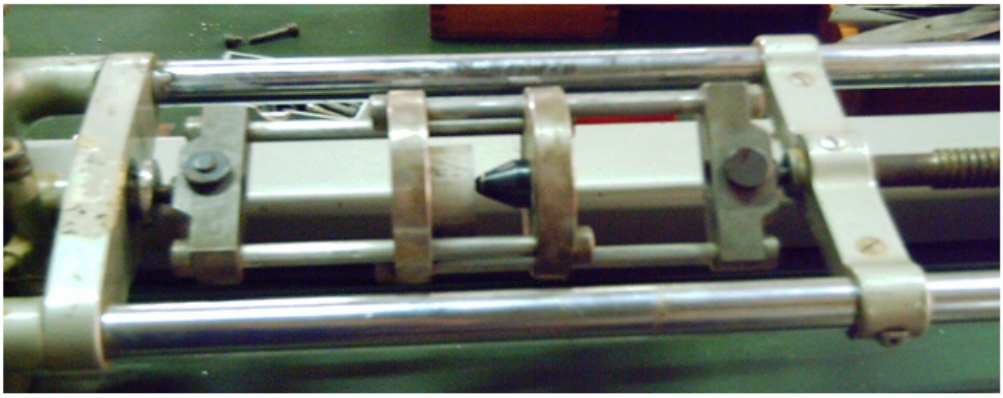

Fig(6) Monsanto tensometer and its compression cage.

Fig.(7) Light section measuring equipment (Microscope BK 70x50)

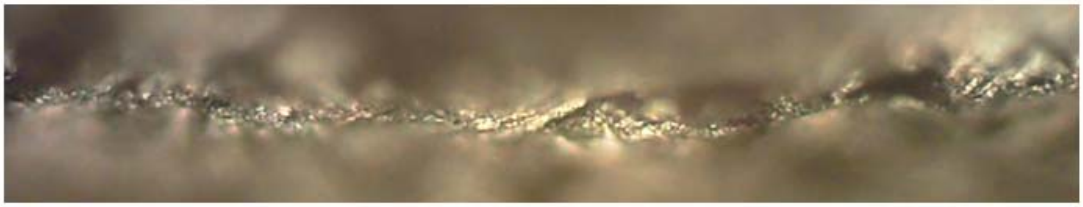

Fig.(8) Profile for Aluminum specimen magnified 375 times by microscope BK 70x50

Fig(9) Image for compression of a spherical indenter of diameter 10mm on a steel specimen to calculate the normal approach, image size 2976x2232 pixels.

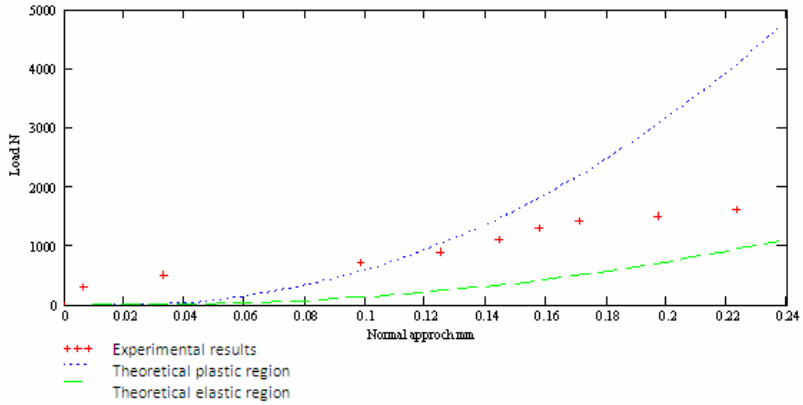

Fig.(10) Relation between applied load and normal approach for aluminum with spherical indenter (D=10mm)

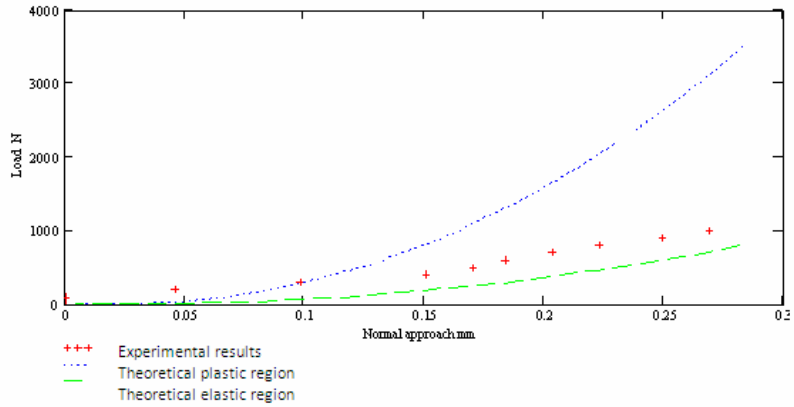

Fig.(11) Relation between applied load and normal approach for aluminum with spherical indenter (D=5mm)

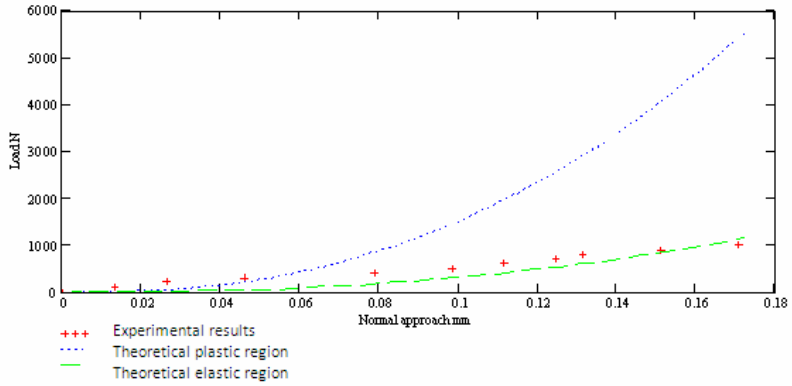

Fig.(12) Relation between applied load and normal approach for Brass2 with spherical indenter (D=10mm)

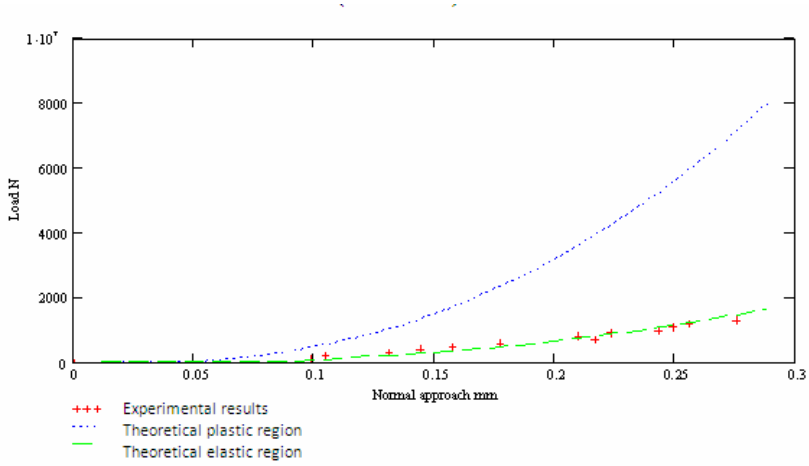

Fig.(13) Relation between applied load and normal approach for Brass2 with spherical indenter (D=5mm)

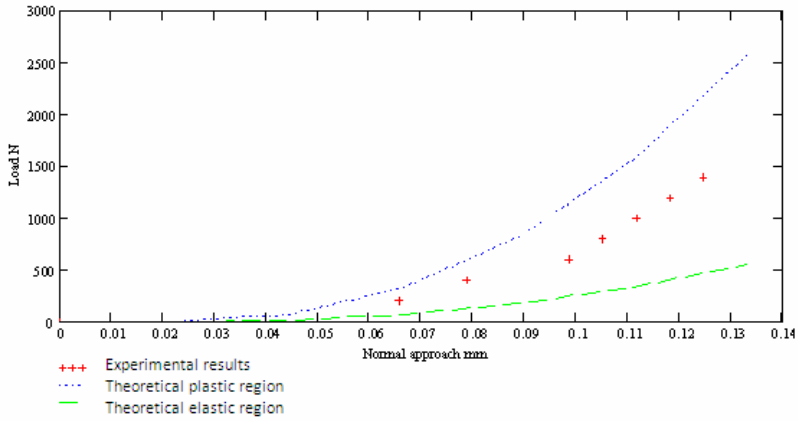

Fig.(14) Relation between applied load and normal approach for Brass1 with spherical indenter (D=10mm)

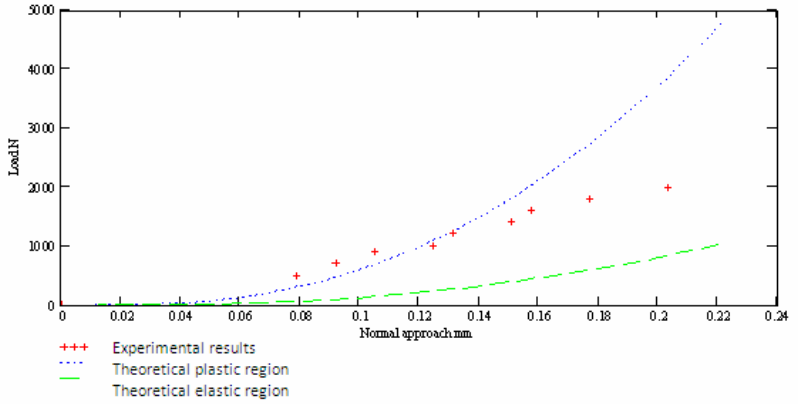

Fig.(15) Relation between applied load and normal approach for Brass1 with spherical indenter (D=5mm)

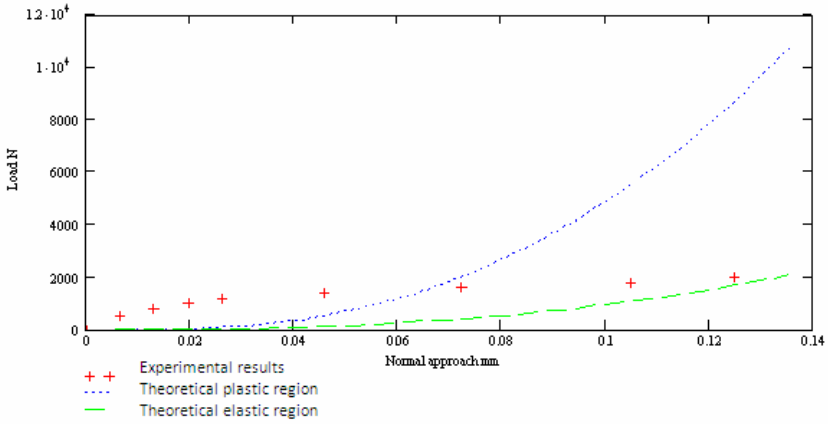

Fig.(16) Relation between applied load and normal approach for steel ck45 with spherical indenter (D=10mm)

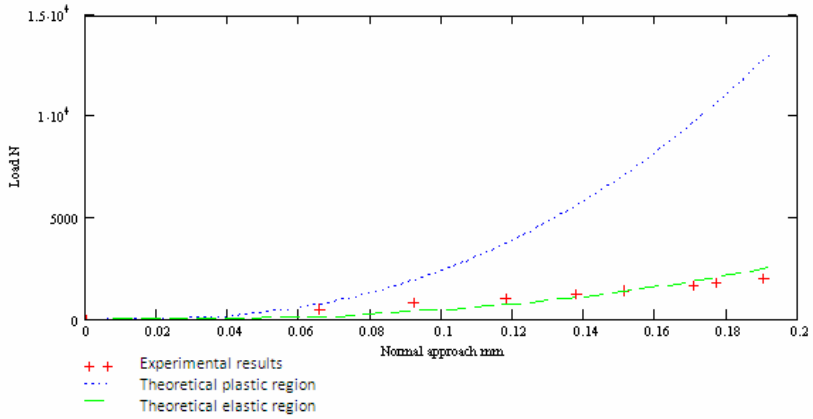

Fig.(17) Relation between applied load and normal approach for steel ck45 with spherical indenter (D=5mm)